A unified view on doping induced evolution of superconductivity and antiferromagnetism in $Ba(Fe_{1-x}Co_x)_2As_2$ single crystals

Lei Fang[1], Huiqian Luo[1], Peng Cheng[1], Zhaosheng Wang[1], Ying Jia[1], Gang Mu[1], Bing Shen[1], I. I. Mazin[2], Lei Shan[1], Cong Ren[1] & Hai-Hu Wen[1]

[1] National Laboratory for Superconductivity, Institute of Physics and Beijing National Laboratory for Condensed Matter Physics, Chinese Academy of Sciences, Beijing 100190, China

[2] Code 6391, Naval Research Laboratory, Washington, DC 20375

Several recently discovered families of FeAs-based high-temperature superconductors share a number of commonalities: the parent phase exhibits an unusual antiferromagnetic (AF) order, while superconductivity is induced by suppressing this order. In most, if not all, these materials the superconducting transition temperature exhibits a dome-like shape versus doping level, in (probably accidental) resemblance of cuprates. In this paper we present systematic measurements of resistivity and Hall effect from undoped to heavily overdoped $Ba(Fe_{1-x}Co_x)_2As_2$ single crystals. The Hall coefficient changes in a systematic way, inconsistent, on the first glance, with the accepted fermiology, as established by calculations and direct measurements. Only at x~0.3, where the hole Fermi surface (FS) disappears in the calculations, and superconductivity disappears in the experiment, does the Hall concentration agree with the formal

doping within the single-band model. Our results strongly suggest that spin-fluctuations due to interband electron-hole scattering play crucial role in superconducting pairing, as well as in the transport relaxation. Doping initially serves to suppress the AF ordering and to reduce the FS gapping; when the suppression is complete, at x~0.08, the critical temperature is maximal. Further doping suppresses spin-fluctuations and weakens the superconductivity.

The recent discovery of high-temperature superconductivity in the FeAs-based system[1] has rekindled the enthusiasm among the researchers. Besides the high critical temperature, a number of intriguing observations vex the minds of scientists: the parent phase exhibits an unusual antiferromagnetic (AF) order,[2] while superconductivity is induced by suppressing this order.[3,4] In the best studied so-called 122 materials superconductivity appears at finite electron *or* hole doping, the transition temperature rapidly rises up to a system-dependent maximum, and then gradually goes down and vanishes. In the 1111 materials the T_c-decrease by overdoping is not always observed, which may be a sample quality issue. Such a dome-like shaped phase diagram is reminiscent of cuprate superconductors. However, there is an increasing body of evidence that here the systematic evolution of the AF order and superconductivity is controlled by rather different physics than in cuprates, where the parent phase is an AF Mott insulator, rather than an AF metal. The cause for the peculiar dome-like shape of T_c vs. doping is still debated.

We have synthesized large high-quality single crystals of $Ba(Fe_{1-x}Co_x)_2As_2$

($0<x<0.3$). We present results of a systematic study of transport properties as we go from undoped to underdoped to heavily overdoped crystals. Our results, especially for the Hall coefficient, seem inconsistent, on the first glance, with the accepted fermiology, as established by first-principles calculations and by direct measurements. They can however, be explained in a two-band model with highly disparate relaxation rates for the electron and hole pockets, and with the carrier concentration substantially reduced in the AF state for all $x<0.08$. Only in severely overdoped samples ($x\sim0.3$) the Hall concentration agrees with the formal doping within the single-band model. At this point, the hole Fermi surface (FS) basically disappears in the calculations, and superconductivity disappears in the experiment. Our results strongly suggest that spin-fluctuations due to inter-pocket electron-hole scattering play crucial role in superconducting pairing, as well as in the transport relaxation.

Based on our transport measurements, a consistent picture of doping evolution emerges. In the undoped compound, AFM ordering opens gaps over the most (up to 90%) of the Fermi surface (FS) area, thus depriving superconductivity of usable carriers. Doping initially serves to suppress AFM ordering; when the suppression is complete, at $x\sim0.08$, no carriers are stolen by the AFM spin-density wave (SDW) any more, and the critical temperature is maximal. Further doping simply suppresses spin-fluctuations and weakens the pairing. This picture is consistent with the idea that at low doping the electron-hole nesting is too good and results in a static magnetism, suppressing superconductivity entirely (at $x<0.04$) or depressing the transition (at $0.04<x<0.08$). Further worsening of the nesting condition slowly weakens the pairing

interaction and leads to an asymmetric dome as observed in the experiment.

Our data suggest two prerequisites for achieving superconductivity: depression (best of all, entire suppression) of the static magnetism ("ungapping" of the FS), and presence of both hole and electron pockets, separated by the AFM wave vector $\{\pi/a,\pi/a\}$. Superconductivity vanished entirely at the doping level where the hole Fermi surface becomes negligibly small. Our results support the picture that the superconductivity is induced by the pairing through inter-pocket scattering of the AF spin fluctuations.[5,6,7]

The main advantage of the (Ba,Sr)Fe_2As_2 system[8] is that it allows fabrication of large single crystals, and can be easily doped with holes (through alkaline metals substitution)[9,10], and with electrons (by substituting Fe with Co),[11,12] in both cases in a very large range of dopings. The dome-like dependence of the critical temperature on doping is particularly well documented for $Ba(Fe_{1-x}Co_x)_2As_2$, where the maximum T_c is about 24 K, reached at x about 0.06-0.10[13-15]. Thermodynamical and transport,[13-15] as well as NMR[16] measurements indicate an intimate relation between the AF order and superconductivity. Therefore we have selected this system for a systematic study.

Single crystal samples were grown by the flux method using FeAs as the flux. The details about the growth and characterization of the crystals are given in the *Methods* Section. In Fig.1 we present the temperature dependence of resistivity of $Ba(Fe_{1-x}Co_x)_2As_2$ single crystals. Here x is the nominal composition of Co used in the crystal growth. Further analysis using the x-ray energy dispersive analysis (EDX) confirmed that the actual concentration of Co in the samples is close to nominal. One

can see that the resistivity drops at about 137 K in the parent phase. This sharp drop of resistivity is attributed to a drastic reduction of the scattering rate in the antiferromagnetic state that overcomes the reduction of the carrier concentration due to partial gapping of the FS[17,18]. We find that the resistivity is 2.5 times smaller at $T \sim 0$ K than at $T = 300$ K (or twice smaller than just above the transition), in agreement with the reduction of optical carrier concentration by a factor of 8 and the relaxation time by a factor of 20[17]. We have verified by first-principles calculations (see Supplementary Material) that *in the fully spin polarized* phase, that is, with the magnetic moment of at least 1.5 μ_B, the calculated Hall concentration $n_h = -n_e = 0.015$, as opposed to 0.15 in the nonmagnetic case, in a quantitative agreement with the above number. Interestingly, a rather small Co doping (2%) turns this sharp drop into an equally sharp (although smaller in magnitude) upturn (Fig. 1). Assuming that the reduction in carrier concentration is comparable to that at $x=0$, we observe that the reduction in the relaxation rate in the AFM state is at least 30% smaller in the 2%-doped samples than in the undoped ones. It is increasingly harder to separate the effect of the FS gapping from that of the relaxation rate, but it is qualitatively clear that the trend continues in the same direction with more doping. Assuming that the main source of the transport relaxation are spin fluctuation, this means that freezing such fluctuations out is more complete when the measured magnetic moments are larger. This is consistent with the "dynamic domains" picture proposed recently[19]. In this picture, local magnetic order is not very sensitive to doping, forming AFM domains at all dopings up to the critical point, and probably even beyond. However, the long range ordered moment is reduced

due to the domain wall motion. The more domain walls freeze at low temperatures, the larger is the ordered moment and the stronger is the reduction of inelastic scattering by the domain walls. This is exactly what we observed in Fig. 1. This is also compatible with fact that the measured reduction in the carrier concentration agrees with the one calculated with full magnetization of Fe ions.

When the doping level reaches 4%, a superconducting transition appears inside the AF phase. The superconducting transition temperature T_c increases quickly with further doping and a maximum T_c is observed at about $x_C = 0.08$. At exactly the same doping the AF/structural transition becomes un-resolvable. Combined with the Hall data discussed below and with the first principle calculation, this suggests a competition between the spin density wave (SDW) and the superconductivity for the density of states at the Fermi level. Only after 8% doping does superconductivity enjoy all carriers and none are stolen by the SDW.

In Figs. 2 and 3 we present the Hall coefficient R_H in wide doping and temperature regimes (in previous works, the Hall effect was measured only at a few doping levels.[15]) The undoped samples provide the first major surprise. By definition, undoped samples are compensated, that is, $n_h = -n_e = n_0$. The general formula for the Hall coefficient in the Boltzmann approximation reads[20]

$$R_H = \frac{\Sigma \sigma_i^2 / n_i^H}{(\Sigma \sigma_i)^2}, \qquad (1)$$

where $\sigma_i = e^2 \left(\frac{n}{m}\right)_i \tau_i$ is the electrical conductivity in the i-th band, $\left(\frac{n}{m}\right) = \frac{\omega_p^2}{4\pi e^2}$ is expressed in terms of the plasma frequency for the relevant crystallographic direction,

and τ_i is the Boltzmann relaxation time. For sufficiently simple (and only for such) Fermi surfaces, the Hall concentration n^{H} differs from the optical concentration n only by sign (for electrons). In the case of fully-compensated semimetals, like undoped pnictides, Eq. 1 reduces to

$$R_H = n_0^{-1} \frac{\sigma_h - \sigma_e}{\sigma_h + \sigma_e} = n_0^{-1} \frac{\mu_h - \mu_e}{\mu_h + \mu_e}, \qquad (2)$$

where $\mu = \sigma/n = \tau/m$ is the mobility. Contrary to a common misconception, the Hall coefficient in compensated or nearly compensated metals is hardly characteristic of the actual carrier concentrations, but is substantially reduced, unless one type of carrier has a much higher mobility than the other. It is therefore most puzzling that in the undoped samples $R_{\mathrm{H}} = -30\times10^{-9}$ m^3/C, corresponding to 0.013 carrier per Fe. Now noticing that (a) the carrier density, obtained in fully polarized (M > 1.6 μ_B/Fe) AF LDA calculation (see *Supplementary Materials*), is n_0=0.015, (b) the calculations strongly overestimate the magnetization, and, correspondingly, should overestimate the FS gapping (*cf*. the even more magnetic GGA calculations in the *Supplementary Materials*), and, (c) the two-band formula has n_0^{-1} as the *upper* boundary for R_H, one appreciates how hard it is to explain the Hall coefficient in the undoped compound in terms of the two-band Boltzmann theory. In principle, assuming an extremely anisotropic ("hot spots"[21]) relaxation rates on the electron pockets one could obtain the desired result. However, as discussed below, at large dopings where hole FSs disappear, the Hall coefficient is quantitatively consistent with a simple one-band picture, suggesting that the two-band, two-relaxation-rates model should be equally good for smaller dopings. Non-Fermi liquid effects, akin to those called up for in connection with the Hall effect in cuprates[22],

cannot be excluded. However one does not expect a separation of the spin and charge degrees of freedom here, nor is the effect the strongest near the critical point. We are left with the conclusion that the actual n_0 is 0.01 or less, and that the transport is dominated by the electrons. This conclusion is supported by the concentration dependence of the low-T Hall coefficient, which reveals a smooth dependence with a sign change around 1.5% hole doping and a maximum of -30×10^{-9} m^3/C around 1.5% electron doping. This can again be reconciled within the same model, using the two-band version of Eq. 1:

$$R_H = \frac{n_h\mu_h^2 + n_e\mu_e^2}{(n_e\mu_e + n_h\mu_h)^2}. \qquad (3)$$

If $\mu_e >> \mu_h$, then $R_H \approx 1/n_e$. However, at the hole doping with an $x \sim n_0$ the electron pocket in the AF state disappears, and the Hall coefficient abruptly changes sign (cf. Fig. 2).

Furthermore, right above the AFM transition R_H is reduced to the value corresponding to a carrier concentration of 0.21 e, a bit larger than the calculated nonmagnetic 0.15e. This is natural and in fact suggests that at this temperature the electron mobility is about 6 times larger than the hole mobility. R_H continues to decrease with the temperature, reaching -0.56×10^{-9} m^3/C at T=300K (-0.56 e/Fe), again consistent with the two-band theory, assuming that now $\mu_h \sim 0.6\mu_e$. To summarize this part, the high-temperature state of $BaFe_2As_2$ is consistent with the nonmagnetic band structure calculations, assuming that the hole mobility is somewhat smaller than the electron mobility. As the temperature is lowered towards the AFM transition, the carrier concentration n_h=-n_e and the *electron* (but not hole) relaxation rate gradually decrease, and both sharply drop below the transition temperature.

Let us now turn to the electron doping. With doping, the explained above, the sharp increase of R_H gets gradually less well expressed, in accordance with the gradual suppression of the magnetism, but is still detectable in all samples where resistivity measurements indicate an AF transition (see Fig.3). As in the undoped crystals, R_H continues to decrease upon heating above T_{AF}, albeit much slower than at low T. This indicates that truly nonmagnetic state for $x<0.08$ is not reached even at room temperature. At higher dopings this effect disappears, and the temperature dependence becomes rather moderate and essentially vanishes above $x>0.2$, as the hole pockets practically close (see *Supplementary materials* for the relevant calculations). The moderate T dependence at $0.08<x<0.2$ is readily understood in terms of somewhat different T dependence of the hole and electron mobilities.

It is also instructive to analyze the Hall coefficient as a function of doping at high temperatures. As the inset of Fig.2 shows, the dependence is nonmonotonic, with three distinct regimes, one for $x<0.04$, the other for $0.04<x<0.08$, and the third for $x>0.08$. In the first regime the effective Hall concentration drops from a rather large number (twice larger than the calculated nonmagnetic n_0) to a number roughly consistent with n_0 at $x=0.04$. In the two-band model that can have but one meaning: the ratio of the hole mobility to the electron mobility sharply decreases with doping (the overall mobility increases, as is clear from the resistivity data discussed in the beginning). The fact that even at 300K the minimal observed Hall concentration is 0.12, smaller than n_0, indicates that fluctuating SDWs are still stealing some carriers even at room temperature. With further doping, however, this effect rapidly diminishes and at $x>0.08$

the measured concentration (at 300K) is consistent with the nominal electron-only concentration calculated from the band structure.

Let us now summarize the picture that evolves from our transport measurements. In the formally stoichiometric, undoped compound at low temperatures transport is dominated by electron pockets. Electron bands have a higher mobility than the hole ones already in the paramagnetic state; the relaxation rate for the electrons (but not that much for the holes) decreases with cooling, and drops precipitously below T_{AF}. Simultaneously, and in full agreement with the optical data, the number of carriers is reduced by nearly an order of magnitude; comparison with the band calculation suggests that the locally ordered magnetic moment of Fe is at least 50% larger than the average static moment in the entire crystal. AFM ordering gaps a large fraction of the FS area, and thus prevents superconductivity.

With doping, gaping becomes less expressed. At x~0.04 there are already enough carriers to support superconductivity, while at x~0.08 the gapping disappears and superconductivity enjoy the full DOS. At high temperatures (T~300 K) the doping dependence at small doping is first dominated by the reduction in the relaxation rate, especially for the holes: at x<0.04 the system still remembers that it was magnetic at low temperatures, follows the same trend in the relaxation rate, and has an effective number of electrons (and holes) smaller than expected in a fully nonmagnetic compound. At x=0.04 the transport is dominated by electrons, and their concentration is still at least 30% smaller than the anticipated nonmagnetic concentration. At 0.04<x<0.08 magnetic effects at 300 K rapidly disappear, causing the effective

concentration to rise back roughly to the calculated nonmagnetic value. At x>0.08 no magnetic ordering effects are seen in the transport, and the measured concentration gradually increases consistently with the doping level.

The Hall coefficient R_H for samples x≥0.04 in wide temperature region is shown in Fig.3. The development of superconductivity from x=0.04 to the maximum at x=0.08 and then gradually disappearing toward x=0.2 is fully consistent with the above picture. In the underdoped regime, T_c is controlled by the gapping of the Fermi surface. Indeed, it was observed[23] that the penetration depth in the underdoped regime follows the same T^2 law, but with an order of magnitude larger prefactor than in the overdoped one. Since λ^2 is inversely proportional to the plasma frequency squared and to (n/m), it is fully consistent with our observation that in the presence of the SDW n is strongly reduced.

In the overdoped regime T_c is controlled by the strength of the available spin fluctuation. The quality of the quasi-nesting between the hole and the electron FSs is reduced with doping, and superconductivity disappears where the hole cylinders disappear at x~0.2. This strongly supports theories explaining superconductivity by nesting-related fluctuations.[5-7] In our present picture, we can naturally explain the asymmetric phase diagram (as shown in Fig.4) in the underdoped and overdoped region because the suppression of T_c is governed by two different mechanisms in these two regions.

The last corollary, very important for theories striving to explain the superconducting properties in pnictides, is that the relaxation rates of holes and

electrons are very disparate. This may be the reason for nonexponential behavior of such characteristics as penetration depth[23] or the NMR relaxation rate.[24,25]. Also, such a possibility needs to be taken into account when analyzing optical spectra (as turned out to be the case in MgB_2[26]). It is worth noting that in order to explain the temperature dependence of the upper critical fields in a 1111 compound within a two-band model one needs at least an order of magnitude (possibly larger) disparity in the mobilities of the two band, even though such an analysis cannot say which band is more mobile[27]. On the other hand, there exist preliminary de Haas-van Alphen data indicating higher mobility of electrons[28].

As a word of caution, our analysis is based on the two-band Fermi liquid theory. Strong non-Fermi-liquid effects, such as spin-charge separation, or strong angular anisotropy of the relaxation rate, may provide alternative interpretation of our Hall data. We do not see, however, good physical reasons for either of these.

References

1. Kamihara, Y., Watanabe, T., Hirano, M. & Hosono, H. Iron-based layered superconductor $La[O_{1-x}F_x]FeAs$ (x=0.05–0.12) with T_c=26 K. *J. Am. Chem. Soc.***130**, 3296–3297 (2008).

2. De la Cruz, C., Huang, Q., Lynn, J. W., Li, J., Ratcliff II, W., Zarestky, J. L., Mook, H. A., Chen, G. F., Luo, J. L., Wang, N. L. & Dai, P. Magnetic order close to superconductivity in the iron-based layered $LaO_{1-x}F_xFeAs$ systems. *Nature* **453**, 899—

902 (2008).

3. Zhao, J., Huang, Q., de la Cruz, C., Li, S., Lynn, J., Chen, W. Y., Green, M. A., Chen, G. F., Li, G., Li Z., Luo J. L., Wang, N. L. & Dai, P. Structural and magnetic phase diagram of $CeFeAsO_{1-x}F_x$ and its relationship to high-temperature superconductivity. *Nature Materials* **7**, 953-959 (2008).

4. Dew, A. J., Niedermayer, Ch., Baker, P. J., Pratt, F. L., Blundell, S. J. , Lancaster, T., Liu, R. H., Wu, G., Chen, X. H., Watanabe, I., Malik, V. K., Dubroka, A., Roessle, M., Kim, K. W., Baines, C. & Bernhard. C. Coexistence of static magnetism and superconductivity in $SmFeAsO_{1-x}F_x$ as revealed by muon spin rotation. *Nature Materials* (in press).

5. Mazin, I. I., Singh. D.J., Johannes, M. D. & Du, M. H. Unconventional sign-reversing superconductivity in $LaFeAsO_{1-x}F_x$. *Phys. Rev. Lett.* **101**, 057003 (2008).

6. Kuroki, K., Onari, S., Arita, R., Usui, H., Tanaka, Y., Kontani, H. & Aoki, H. Unconventional pairing originating from disconnected Fermi surfaces in superconducting $LaFeAsO_{1-x}F_x$. *Phys. Rev. Lett.* **101**, 087004 (2008).

7. Wang, F., Zhai, H., Ran, Y., Vishwanath, A. & Lee, D.-H. Functional renormalization-group study of the pairing symmetry and pairing mechanism of the

FeAs-based high-temperature superconductor. *Phys. Rev. Lett.* **102**, 047005 (2009).

8. Rotter, M., Tegel, M. & Johrendt, D. Superconductivity at 38 K in the iron arsenide $(Ba_{1-x}K_x)Fe_2As_2$. *Phys. Rev. Lett.* **101**, 107006 (2008).

9. Ni, N., Bud'ko, S. L., Nandi, S., Rustan, G. E., Goldman, A. I., Gupta, S., Corbett, J. D., Kracher, A. & Canfield, P. C. Anisotropic thermodynamic and transport properties of single-crystalline $Ba_{1-x}K_xFe_2As_2$ (x = 0 and 0.45). *Phys. Rev. B* **78**, 014507 (2008).

10. Luo, H.-Q., Wang, Z.-S., Yang, H., Cheng, P., Zhu, X. & Wen, H.-H. Growth and characterization of $A_{1-x}K_xFe_2As_2$ (A = Ba, Sr) single crystals with x=0-0.4. *Supercond. Sci. Technol.* **21**, 125014 (2008).

11. Sefat, A. S., Jin, R., McGuire, M. A., Sales, B. C., Singh, D. J. & Mandrus, D. Superconductivity at 22 K in Co-doped $BaFe_2As_2$ crystals. *Phys. Rev. Lett.* **101**, 117004 (2008).

12. Cao, G., Wang, C., Zhu, Z., Jiang, S., Luo, Y., Chi, S., Ren, Z., Tao, Q., Wang, Y. & Xu, Z. Superconductivity induced by cobalt doping in iron-based oxyarsenides. *Phys. Rev. B* 79, 054521 (2009).

13. Ni, N., Tillman, M. E., Yan, J.-Q., Kracher, A., Hannahs, S. T., Bud'ko, S. L. &

Canfield, P. C. Effects of Co substitution on thermodynamic and transport properties and anisotropic H_{c2} in $Ba(Fe_{1-x}Co_x)_2As_2$ single crystals. *Phys. Rev. B* **78**, 214515 (2008).

14. Chu, J.-H., Analytis, J. G., Kucharczyk, C. & Fisher, I. R. Determination of the phase diagram of the electron doped superconductor $Ba(Fe_{1-x}Co_x)_2As_2$. *Phys. Rev. B* **79**, 014506 (2009).

15. Wang, X. F., Wu, T., Wu, G., Liu, R. H., Chen, H., Xie, Y. L. & Chen, X. H. Abnormal T-linear susceptibility and Phase diagram of $BaFe_{2-x}Co_xAs_2$ single crystals. *arXiv*: 0811.2920 (2008).

16. Ning, F. L., Ahilan, K., Imai, T., Sefat, A. S., Jin, R., McGuire, M. A., Sales, B. C. & Mandrus, D. ^{59}Co and ^{75}As NMR investigation of electron-doped high T_c superconductor $BaFe_{1.8}Co_{0.2}As_2$ (T_c = 22 K). *J. Phys. Soc. Jpn*. **77,** 103705 (2008).

17. Hu, W. Z., Dong, J., Li, G., Li, Z., Zheng, P., Chen. G. F., Luo, J. N. & Wang, N. L. Origin of the spin density wave instability in AFe_2As_2 (A=Ba, Sr) as revealed by optical spectroscopy. *Phys. Rev. Lett.* **101**, 257005 (2008).

18. Tropeano, M., Fanciulli, C., Ferdeghini, C., Marre', D., Siri, A.S., Putti, M., Martinelli, A., Ferretti, M., Palenzona, A., Cimberle, M. R., Mirri, C., Lupi, S., Sopracase, R., Calvani, P., Perucchi, A. Transport and infrared properties of

SmFeAs($O_{1-x}F_x$): from SDW to superconducting ordering, *Supcond. Sci. Tech.* **22**, 034004 (2009).

19. Mazin, I. I., Johannes, D. M. A key role for unusual spin dynamics in ferropnictides, *Nature Physics* **5**, 141 (2009).

20. Ashcroft, N. W., & Mermin, N. D. *Solid State Physics*, Edition 1976, Thompson Learning, Inc.

21. A.T. Zheleznyak, V.M. Yakovenko, H.D. Drew, and I.I. Mazin,, Phenomenological interpretations of the ac Hall effect in the normal state of $YBa_2Cu_3O_7$, *Phys. Rev.* **B57**, 3089 (1998).

22. P.W. Anderson, Hall effect in the two-dimensional Luttinger liquid, *Phys. Rev. Lett.* **67**, 2092 - 2094 (1991)

23. R. T. Gordon, C. Martin, H. Kim, N. Ni, M. A. Tanatar, J. Schmalian, I. I. Mazin S. L. Bud'ko, P. C. Canfield, and R. Prozorov, The London penetration depth in single crystals of $Ba(Fe_{1-x}Co_x)_2As_2$ at various doping levels, *Phys. Rev. B* - Rapid Comms, in press.

24. Nakai, Y., Ishida, K., Kamihara, Y., Hirano, M., Hosono, H. Evolution from Itinerant

Antiferromagnet to Unconventional Superconductor with Fluorine Doping in $LaO_{1-x}F_xFeAs$ Revealed by ^{75}As and ^{139}La Nuclear Magnetic Resonance, *J. Phys. Soc. Jap.* **77**, xxx (2008).

25. Matano, K., Ren, Z.A., Dong, X.L., Sun, L.L., Zhao, Z.X., Zheng, G. Q. Spin-singlet superconductivity with multiple gaps in $PrO_{0.89}F_{0.11}FeAs$, *Europhys. Lett.* **83**, 57001 (2008).

26. Kuz'menko, A.B., Mena, F.P., Molegraaf, H.J.A., van der Marel, D., Gorshunov, B., Dressel, M, Mazin, I.I. , Kortus, J., Dolgov, O.V., Muranaka, T., Akimitsu, J., Manifestation of multiband optical properties of MgB_2, *Solid State Comm.*, **121**, 479-494 (2002).

27. Upper critical fields and thermally-activated transport of NdFeAsO0.7F0.3 single crystal, J. Jaroszynski, F. Hunte, L. Balicas, Youn-jung Jo, I. Raičević, A. Gurevich, D. C. Larbalestier, F. F. Balakirev, L. Fang, P. Cheng, Y. Jia, and H. H. Wen, *Physical Review* **B 78**, 174523 (2008)

28. A. I. Coldea, private communication.

29. Pfuner, F., Analytis, J.G., Chu, J.-H., Fisher, I.R., and Degiorgi, L., Charge dynamics of the spin-density-wave state in $BaFe_2As_2$, *arXiv:0811.2195* (2008).

Acknowledgements

We thank Chandra Varma, Tao Xiang and Junren Shi for valuable discussions. This work was supported by the Natural Science Foundation of China, the Ministry of

Science and Technology of China (973 Projects No.2006CB601000, No. 2006CB921802), and Chinese Academy of Sciences (Project ITSNEM). I.I.M. was supported by the U.S. Office of Naval Research.

Authors contributions:

All requirements for materials and samples should be addressed to Hai-Hu Wen at hhwen@aphy.iphy.ac.cn. IIM performed the calculations and contributed to interpretation. LF and PC made the $Ba(Fe_{1-x}Co_x)_2As_2$ crystals, LF made most of the measurements in this paper. HQL and ZSW made the $Ba_{1-x}K_xFe_2As_2$ crystals and measured the transport properties.

Competing financial interests

The authors declare that they have no competing financial interests.

Figure Captions

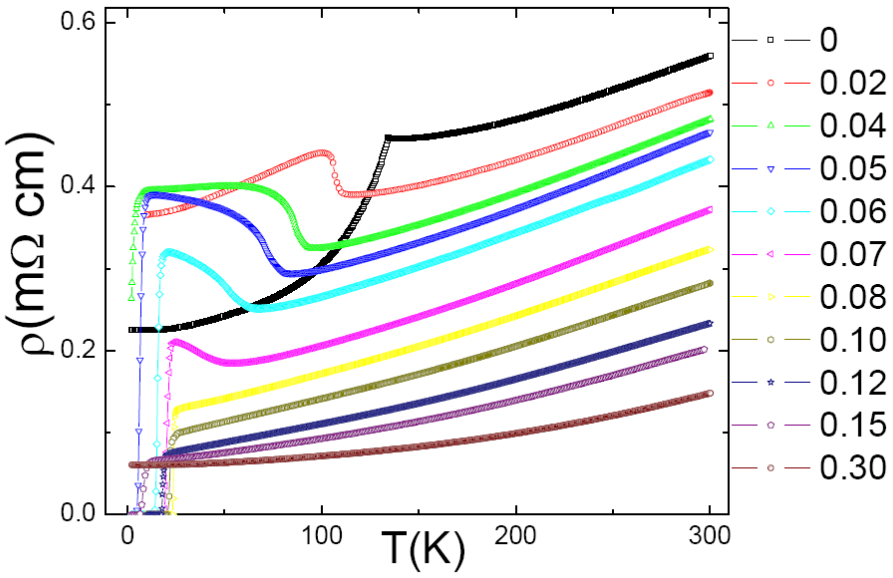

Figure 1 Temperature dependence of resistivity of $Ba(Fe_{1-x}Co_x)_2As_2$ single crystals. One can see that the resistivity drops at about 137 K in association of the AF/structural transition in the parent phase. This anomaly evolves into an uprising of resistivity at a doping level of only 2 %. A low doping level of only 4 % already induces superconductivity. The AF/structural transition temperature quickly drops down with doping. The maximal superconducting transition temperature occurs at about 25.2 K with a doping level of 8 %, where the AF/structural transition cannot be explicitly resolved.

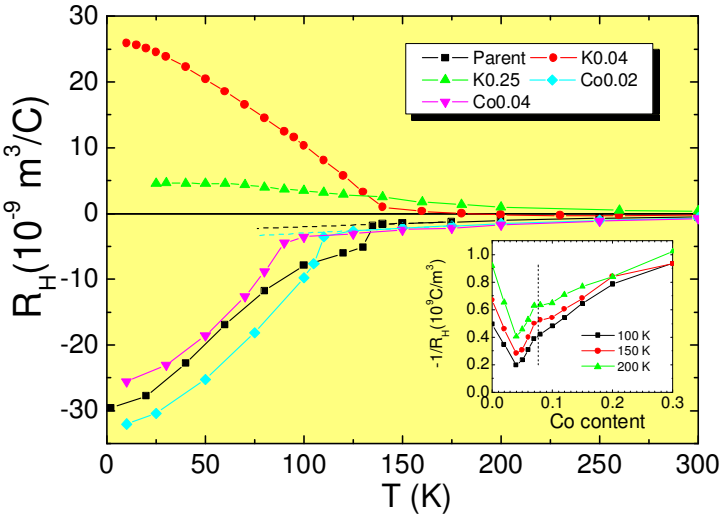

Figure 2 The temperature dependence of R_H for the parent phase (squares), 4% (circles) and 25 % (up-triangles) K-doped $Ba_{1-x}K_xFe_2As_2$ crystals, 2% Co-doped (diamond) and 4 % Co-doped (down-triangles) $Ba(Fe_{2-x}Co_x)_2As_2$ crystals. Note that a very small K doping leads to a sudden sign change of R_H in the AF state. The inset shows the doping dependence of $-1/R_H$ in the normal state at three different temperatures (note that the unit cell volume of $BaFe_2As_2$ is 101.5 Å^3, so that $n^H=0.137\times10^{-9}/R_H$ e/Fe). One can distinguish three regimes: initially $-1/R_H$ drops sharply with doping, reaches a minimum at x=4%, then rapidly rises again. At $x_c = 0.08$ there is a visible change of slope, marked by the vertical dashed line that corresponds to the maximum T_c and vanishing of the AF order.

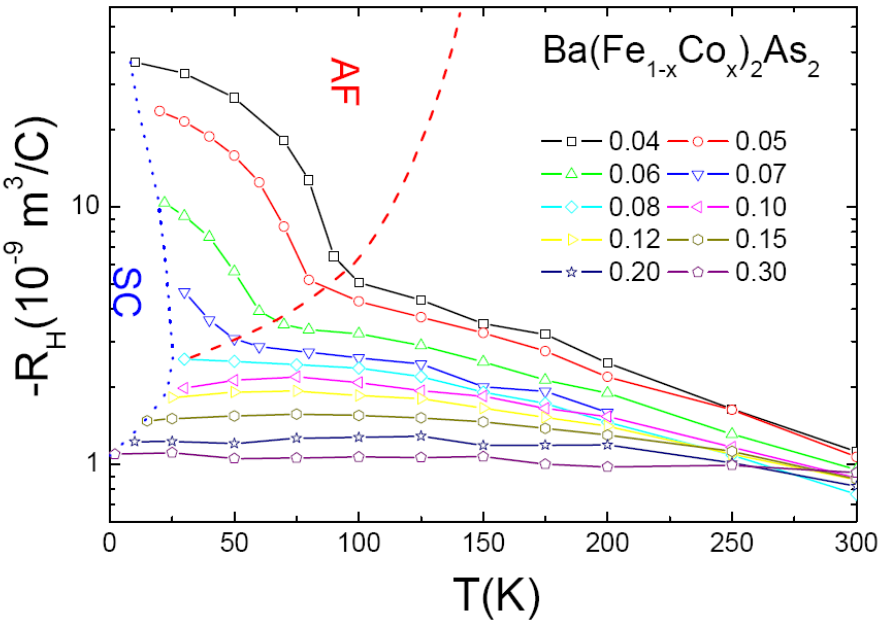

Figure 3 Temperature dependence of Hall coefficient R_H measured at 9T. At a low doping level ($x \leq 0.07$), there is a clear transition point T_{AF} (the red dashed line) below which the value of R_H rises sharply, indicating a dramatic change of the carrier number and scattering rate, as discussed in the text. In the normal state, $|R_H|$ decreases with temperature. In the strongly overdoped regime transport is dominated by a single electron band, the temperature dependence becomes much weaker and even vanishes at x=0.30, and the absolute value of the Hall concentration becomes equal to x. The blue dotted line outlines the superconducting region. In the underdoped region, superconductivity and a long range AF order seem to co-exist, with the former emerging stronger as the latter is suppressed.

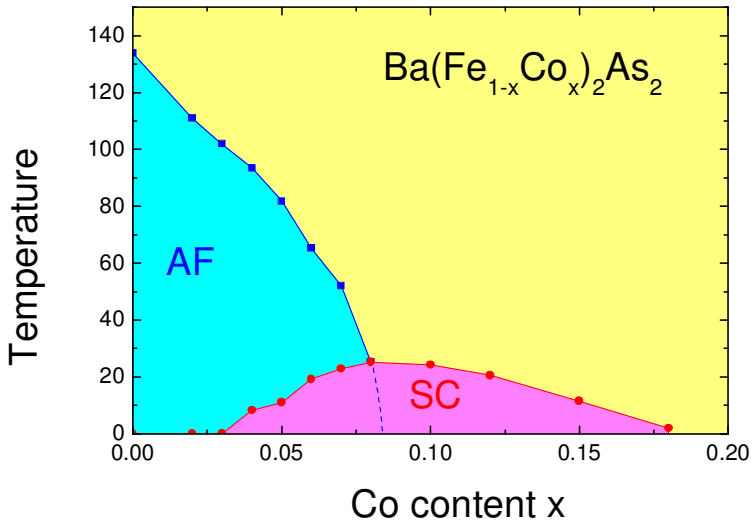

Figure 4. The phase diagram derived from the resistivity and Hall effect measurements. The superconducting transition temperature T_c is defined according to the 95% ρ_n criterion. The superconducting dome is asymmetric with a steeper ramping up slope in the underdoped region. The AF/structural transition temperature crosses T_c at $x_c \sim 0.08$. In the underdoped region the superconductivity and the AF order apparently coexist .

Supplementary Materials.

Methods

I. **Crystal growth**

The crystals were grown by self-flux method using FeAs as the flux. High purity (99.9%) Barium flakes were mixed with thoroughly grounded FeAs and CoAs powders according to the stoichiometric ratio Ba : FeAs : CoAs = 1: 4(1-*x*): 4*x*. The mixture was compressed into pellets at a pressure of about 8 MPa. Then a pellet was put into an Al_2O_3 crucible with high purity and sealed in an evacuated quartz tube. To avoid oxidation, weighing and mixing were performed in a glove box (with H_2O and O_2 both below 0.1 ppm). The sealed quartz tube was put into a muffle furnace. Initially the furnace was warmed up to 900 ^oC and kept at this temperature for 10 hours. Then the temperature was increased to 1150~1170 ^oC at a rate of 100 ^oC/h and kept at this value for about 5 hours. Subsequently the furnace was slowly cooled to 900 ^oC at a rate of 3~5 ^oC/h. Empirically a slower cooling rate, for example 3 ^oC/h, was improving the crystal quality, such as homogeneity and the diamagnetic superconducting transition width. Finally the furnace was cooled to the room temperature at a rate of 50 ^oC/h to relieve the inner stress in crystals. The obtained ingots were normally consisting of $Ba(Fe_{1-x}Co_x)_2As_2$ single crystals and solidified flux. Typically the resulted single crystals had considerable sizes with dimension up to 8×5×1 mm^3. Due to a weak contamination of FeAs flux, the outer layers of single crystals were cleaved and discarded; and the rest was used for the transport

measurements.

II. Measuring and characterization of the Hall coefficient R_H

Sample crystallization was checked by the X-ray diffraction (XRD) based on an M18AHF diffractometer (MAC Science) and a JEOL 2010 high-resolution electron microscope operated at 200 kV. Crystal morphology and composition and chemical homogeneity were checked by scanning electron microscope (Oxford) and energy dispersive X-ray microanalysis (EDX). The diamagnetic superconducting transition was measured by a vibrating sample magnetometer (VSM) based on a physical property measurement system (PPMS of Quantum Design) with the magnetic field perpendicular to the ab plane of the crystals. The measurements of in-plane longitudinal (ρ_{xx}) and transverse (ρ_{xy}) resistances were carried out in PPMS using the standard six probe method. By sweeping the magnetic field at a fixed temperature both ρ_{xx} and ρ_{xy} could be obtained at the same time. The Hall coefficient R_H was calculated as $R_H=\rho_{xy}/H$ at $H = 9$ T. The thickness of each crystal was carefully measured through a gauge integrated into an optical microscope, the smallest scale of the gauge is 25 μm. In the Figure 1 of this supplementary material, we show an example of characterization of our crystals.

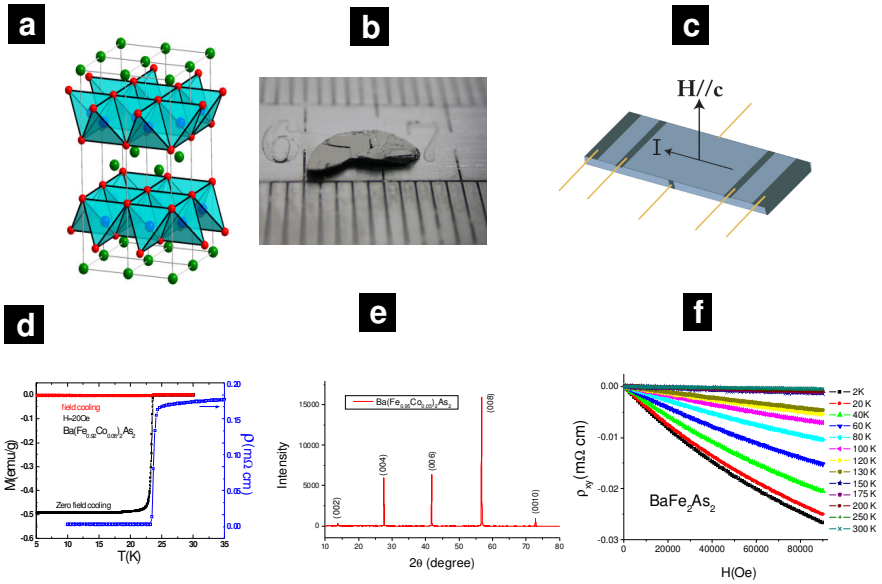

Figure-1 (Supplementary) **a** Crystal structure of $Ba(Fe_{1-x}Co_x)_2As_2$. **b** A typical as-grown sample before shaping it for the measurements. **c** The measurement configuration for both resistivity and Hall effect. **d** Temperature dependence of the magnetization and resistivity for a sample with x=0.08. **e** X-ray diffraction for the sample x=0.05. **f.** Raw data of the Hall resistivity ρ_{xy} for the undoped sample, Hall coefficient is determined through $R_H=\rho_{xy}/H$ (at 9T).

III. Electronic structure calculations

All calculations were performed using the Full Potential LAPW method as implemented in the WIEN2k package. The experimental crystal structure for $BaFe_2As_2$ was used for all calculations. Doping was taken into account through the rigid band approximation. The same setup was used as in Ref. 5.

In Fig. 2 (Supplementary) we compare the nonmagnetic Fermi surface for the undoped compound with the magnetic one (using an LDA exchange-correlation functional, magnetic moment 1.6 μ_B/Fe). Note the destruction of the large 2D cylinders that are reduced to small 3D pockets. In the same figure we show the Fermi surfaces calculated at x=0.2 and x=0.3, in the rigid band model. Note how at x=0.2 the hole pockets loose their 2D character (and 2D nesting) and practically disappear at x=0.3.

Fig. 3 (Supplementary) shows the calculated volumes of the hole and electron pockets as a function of electron doping, in the rigid band approximation.

Fig. 4 (Supplementary) illustrates the point made in the text, that at room temperature for x>0.08 the measured Hall concentration is roughly consistent with the calculated carrier concentration. The calculations used the pocket volumes shown in Fig. 3, assuming an x-dependent ratio of the electron and hole mobilities, $\mu_e/\mu_h=1.3x$.

Finally, in Table 1 (Supplementary) we show the calculated transport parameters. To get the reader an idea of how the Fermi surface gapping increases with the exchange splitting, we show the results for two different exchange-correlation functionals: less magnetic LDA and more magnetic GGA. One can see drastic decrease in the number of carrier in the calculated AFM state as opposed to the nonmagnetic state, as well as the sensitivity to the calculated magnetic moment. Note that even the less magnetic LDA calculation still gives a much larger magnetic moment than the experimentally observed one (less than 1 μ_B), an effect usually ascribed to spin fluctuations. It is worth noting that the experimentally measured plasma frequency at room temperature is 1.6[17] to 1.7[29] eV, corresponding to an optical mass renormalization of 2.4 to 2.7.

Deleted: 7

Table 1. (Supplementary) Calculated transport parameters of undoped $BaFe_2As_2$ in the magnetic and nonmagnetic case (the low-temperature experimental crystal structure was used). As discussed in the text, n_0 is both concentration of the electron and of the holes, and $\omega_p^2=4\pi e^2(n/m)$. The relative contribution of electrons and holes to the in-plane nonmagnetic ω_p^2 is 1.3:1, due to different optical effective masses (not to be confused with the effective mass at the Fermi level, as measured, for instance, by quantum oscillations), which also contributes to a difference in mobilities. The coordinate system is selected in such a way that *x* is along the longer Fe-Fe bond and *y* is along the shorter one. Two different entries for the magnetic case corresponds to the LDA (M=1.66 μ_B) and GGA (M=2.05 μ_B) calculations. For the nonmagnetic calculations, the results for LDA and GGA are very similar.

M, μ_B/Fe	n_0, e/Fe	ω_{px}, eV	ω_{py}, eV	ω_{pz}, eV
0	0.15	2.63	2.63	0.78
1.66	0.015	0.83	0.85	1.14
2.04	0.005	0.78	0.67	1.05

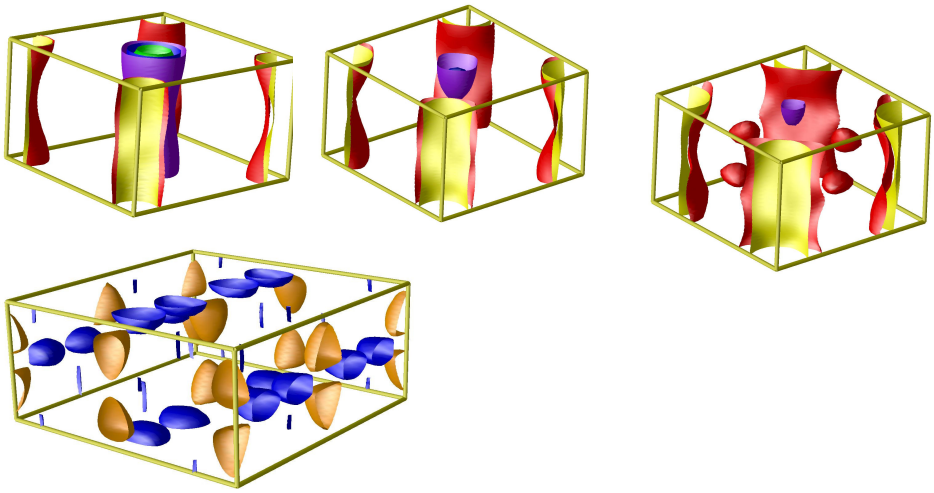

Figure 2. (Supplementary) Fermi surfaces calculated for nonmagnetic $Ba(Fe_{1-x}Co_x)_2As_2$ for x=0, 0.2 and 0.3 (in the virtual crystal approximation), and for the fully polarized (LDA calculations, M=1.66 μ_B/Fe) $BaFe_2As_2$ (the same volume in the reciprocal space is shown as in the previous three pictures).

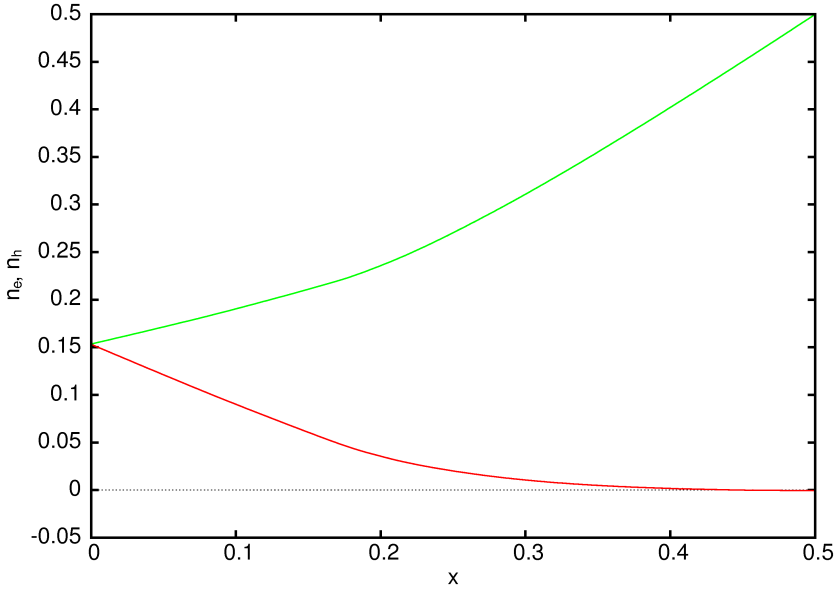

Figure 3. (Supplementary) The calculated volumes of the hole and electron pockets as a function of electron doping.

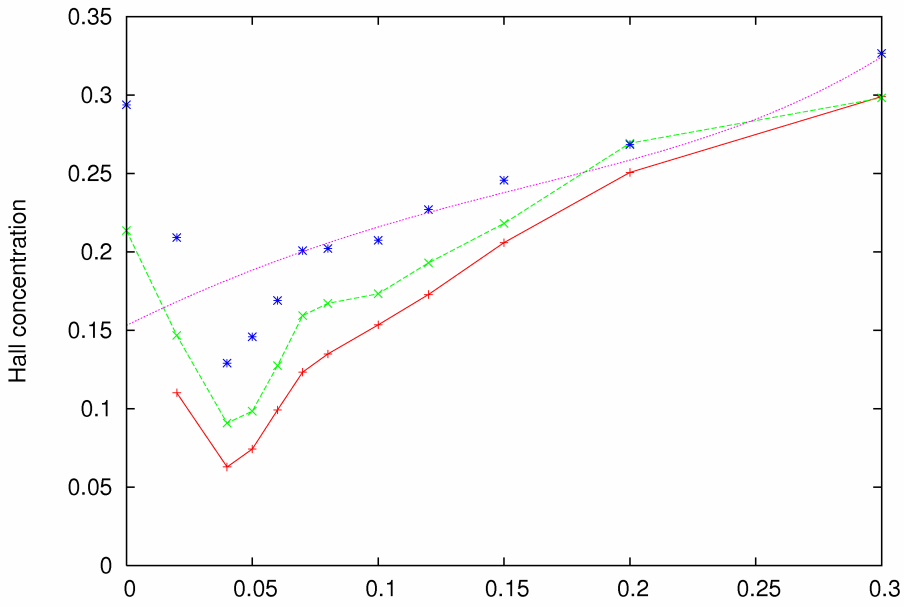

Figure 4. (Supplementary) Electron concentration extracted from the Hall coefficient presented in the main text (Fig. 2 inset), as compared with the calculated Hall concentrations, as described in the text.